Sustainable Energy & Fuels

In-Depth Understanding of the CO_2 Limitation of Air Fed Anion Exchange Membrane Fuel Cells

Journal:	*Sustainable Energy & Fuels*
Manuscript ID	SE-ART-12-2019-001212
Article Type:	Paper
Date Submitted by the Author:	07-May-2019

Complete List of Authors:	Divekar, Ashutosh; Colorado School of Mines Neyerlin, Ami; NREL Antunes, Christopher; NREL Strasser, Derek; NREL Motz, Andrew; Colorado School of Mines Seifert, Sönke; Argonne National Laboratory Zuo, Xiaobing; Argonne National Laboratory Pivovar, Bryan; National Renewable Energy Laboratory Herring, Andrew; Colorado School of Mines, Chemical and Biological Engineering

ARTICLE

In-Depth Understanding of the CO_2 Limitation of Air Fed Anion Exchange Membrane Fuel Cells

Received 00th January 20xx,
Accepted 00th January 20xx

DOI: 10.1039/x0xx00000x

www.rsc.org/

Ashutosh G. Divekar,[a] Ami C. Yang-Neyerlin,[b] Christopher M. Antunes,[b] Derek J. Strasser,[b] Andrew R. Motz,[a] Soenke S. Seifert,[c] Xiaobing Zuo,[c] Bryan S. Pivovar,[b] and Andrew M. Herring[a*]

The interaction of a perfluorinated anion exchange membrane(AEM), initially in the hydroxide form, with atmospheric CO_2 at 60 °C and under a range of relative humidities is studied both in a fuel cell and with ex-situ measurements to understand the performance drop. A new novel titration method was used to quantify the amounts of hydroxide,carbonate and bicarbonates in the membrane. However, hydroxide and bicarbonate react internally which disturbs the equilibrium and hence it's impossible to detect real species concentration using titration. The uptake of CO_2 leads to a rise in membrane mass within the first 15 min. The anionic conductivity of the AEM experiences a quick drop within 20 minutes to carbonate, bicarbonate level. However, switching the inlet gas to 0 ppm CO_2 reverses the equilibrium due to desorption phenomenon. Investigating the morphology of the film by small angle x-ray scattering shows that the ionomer domains looses intensity as the reaction progresses, the drop is of the double-exponential type but the time of equilibration is slower when compared to that of the conductivity. The wide-angle x-ray scattering data was fit to 3 gaussian peaks showing that the CF_2 inter-chain spacing becomes less crystalline during the process. 30% of peak power was lost for this membrane in an AEM fuel cell on addition of CO_2, yet we observed the highest H_2/ambient air(400 ppm CO_2) performance, 446 mW/cm^2 reported to date.

Introduction

Anion exchange membranes (AEMs) are a promising technology to enable a wide variety of electro-chemical conversion technologies, e.g., fuel cells, electrolysis, photo-electrocatalytic water splitting, or electro-dialysis. They offer potential advantages over proton exchange membrane fuel cells (PEMFCs) which include, facile oxidation kinetics, low-fuel cross-over, and most importantly potentially no reliance on precious metal (e.g. Pt) catalysts in the electrodes. In an AEM fuel cell (AEMFC) an oxidant flows through the cathode compartment where it is reduced to form the OH^- charge carrier.[1]

In the early years of development, the H_2/O_2 AEMFC performance that were reported were typically <100 mW/cm^2.[2, 3] The OH^- anion conductivity in these studies was very low and hence many researchers worked on development of new polymer chemistries (different backbone or cation group) to obtain a highly OH^- conductive membrane. However, since 2015, this problem seems to have been solved with many AEMs showing ionic conductivity above 100 mS/cm.[4] Therefore, the remaining challenges are an understanding of the rational catalyst design for best performances, developing chemistries with advanced cations, and mitigating the performance loses due to carbon-dioxide absorption.

One of the major challenges of using ambient air as an oxidant in an AEMFC is that the CO_2 reacts with the OH^- charge carrier to produce both HCO_3^- & CO_3^{2-} which reduces the performance of the AEM. This reaction leads to a loss of the net ionic mobility, which directly affects the conductivity of the membrane and hence produces a loss in performance of the fuel cell. In the AEM membrane electrode assembly (MEA) in the fuel cell, it should be noted that O_2 gets reduced directly to form OH^- which then reacts with absorbed CO_2 to form CO_3^{2-}. Additionally it should also be noted that the CO_2 gets reduced with O_2 to form CO_3^{2-}.[5, 6] Recently, it was reported that the performance of an AEMFC is approaching the state-of-the art PEMFC performance.[7] But, here it should be noted that typically AEMFC performance is recorded with pure O_2 or CO_2 free air as the oxidant.[8] H_2/air AEMFC performances has been summarized by Ziv et. al.[8] The best peak power performance was reported by Li et al. as 320 mW/cm^2.[9]

In 2013 it was proposed to operate AEMFCs at temperatures above 80 °C to avoid the carbonation problem, due to reduced solubility of CO_2 in the membrane as per Henry's law.[10] At the time

[a] *Colorado School of Mines*
[b] *National Renewable Energy Laboratory*
[c] *Advanced Photon Source, Argonne National Laboratory*
Corresponding author: Prof. Andrew Herring (aherring@mines.edu)†
Footnotes relating to the title and/or authors should appear here.
Electronic Supplementary Information (ESI) available: [details of any supplementary information available should be included here]. See DOI: 10.1039/x0xx00000x

few AEMs were stable at these conditions,[11] but much progress in AEM technologies has allowed AEMFC operation at 80 °C.[4] Our data that we recently published, suggests that the carbonation is still significant at 80 °C.[12] It also suggests that carbonation is reduced at lower CO_2 concentrations. The strategy of reducing the CO_2 concentrations was implemented by CellEra/Elbit Inc, where they fit a regenerative CO_2 filter before the air inlet to reduce the CO_2 concentration from 400 ppm to <5 ppm.[10, 13] The air filter is also a suggested strategy for the Li-air battery (with automobile applications) where CO_2 reaction with Li analogously affects the performance.[10, 14] To further improve the performance of the AEMFC in ambient air operation, and remove the additional unit operation of a CO_2 filter, it is necessary to understand the influence of CO_2 on the membrane properties.

Very few attempts have been made to understand the effects of this reaction on all membrane characteristics. Primarily researchers have investigated the concentration profile of the products of the CO_2 reaction with OH^- ions using a titration technique.[15-18] The Tokuyama data suggests that the CO_3^{2-} ions are the only species that are generated while OH^- ions remain in the membrane and once they get depleted the concentration of HCO_3^- rises.[15] However, we should also note here that the authors only used the Warder titration method, see below, which has only two end-points which is not sufficient to evaluate the concentration of three species simultaneously.[19] Therefore, we used a more sophisticated titration methodology, described below, which can evaluate the concentrations of all three species.

Previous literature suggest that the total ionic conductivity of an anion exchange membrane reduces as the fraction of OH^- is depleted and the carbonates increases.[18] As the membrane is exposed to air containing 400 ppm CO_2, the ionic conductivity value drops over time due to formation of carbonate and bicarbonate. The HCO_3^-/CO_3^{2-} ions have ~4 times lower mobility in an infinite dilution of H_2O.[1] The OH^- ion can also conduct via the Grotthus hoping mechanism whereas HCO_3^-/CO_3^{2-} ions cannot Grotthus hop therefore they have lower ionic mobilities.[11, 20] However, the actual number of the ionic mobility is different in an AEM system, because of the interaction of the ions with the polymer chain and the tortuosity.[8, 21] Also, the size of the HCO_3^-/CO_3^{2-} ions is larger than OH^-.[22] Myles et al. have used modelling of the concentration profile to study the transient conductivity data of the Tokuyama A201 and the ETFE grafted AEMs.[23] The authors have suggested that the drop in conductivity happens in two regions: hydroxide depletion and carbonate-bicarbonate exchange. From their data we notice that the A201 approaches equilibrium in ~30 min whereas ETFE takes ~50 min. The different times are attributed to the difference in hydration, morphology and chemical composition. Pandey et al. have studied transient conductivity of ETFE grafted AEM,[24] where the data was fit to a single exponential decay.

To date most of articles only studied the CO_2 reaction in AEMs in conjunction with limited membrane properties.[15, 17, 24-26] Here for the first time we build a comprehensive picture of the effect of CO_2 uptake on membrane properties in an perfluorinated AEM (PFAEM). The PF polymer in this study was synthesized from a perfluorinated sulfonyl fluoride ionomer precursor (EW 798) developed by 3M (USA). This PFAEM is a co-polymer of tetrafluoroethylene (PTFE) and a trifluoroethylene functionalized with a perfourinated sulfonyl fluoride 4 carbon chain. Detailed synthesis and characterization of this polymer has been reported by Park et. al. and Divekar et. al. respectively.[27, 28]

We performed the measurements at a constant temperature of 60 °C and varying relative humidity conditions. Ultimately, the goal of this study was to understand the CO_2 limitation on AEMs from many angles so strategies can be proposed to mitigate the problem in an actual H_2/Air fuel cell system. From the knowledge gained in this work we were able to demonstrate a fuel cell performance using H_2/ambient air (400 ppm CO_2) of 446 mW/cm^2, the highest reported to date.

Experimental

Materials

The 6 carbon-spacer chained perfluorinated anion exchange polymer was supplied in the chloride form by the National Renewable Energy laboratory, Golden, CO.[28] Potassium hydroxide (KOH), Sodium chloride (NaCl) were purchased from Fischer-Scientific., Phenolphthalein & methyl orange indicators from Fischer-Scientific. Pure 1N KOH and extra-pure deionized water from Across chemicals. Ultra-high purity Ar, N_2, and zero-grade compressed air (400 ppm CO_2) was obtained from General Air Corporation. House air with (CO_2<3ppm) was generated on-site.

Membrane Formation

AEMs were fabricated by dissolving and stirring the PFAEM polymer in dimethylacetamide (DMAc) at 120 °C for a minimum 2 h to make 5-10 wt.% solutions.[14] The solution was drop cast on a Teflon sheet, followed by drying in an oven at 60 °C to form membranes of thickness ca. 50 µm. The membranes were then annealed at 160 °C and 800 psi for 10 min.

Controlled exposure of samples to environmental conditions

Samples were exchanged to the pure OH^- form by soaking the Cl^- form samples in 1M KOH solution three times for 24 h and washing the samples with degassed DI water in a CO_2 free N_2 glove-bag four times. The samples were kept in an air-tight container with salt solutions (NaBr, KCl, KNO_3) to maintain specific humidity condition (50,75,85%RH) locally before being transferred to an environmental chamber (Test Equity) under ambient air.[29] The chamber was kept at a fixed temperature of 60 °C and varied relative humidity (%RH). The experiments were performed at %RH of 50, 75, or 85. The samples were exposed to these conditions and taken out at various times to determine the concentration profile. After exposure, the samples were soaked in 1M KCl solution for 24 h and then the titration

methodology described below was followed to evaluate the concentration profile.

Titration methodology

To determine OH^-, CO_3^{2-}, and HCO_3^- simultaneously we used a method consisting of three titrations.

1.The Warder method[19] is used to determine the total anion content in the membrane, as described below.

$$OH^- + HCl \xrightarrow{phenolphthalein} H_2O + Cl^- \quad (1)$$

$$CO_3{}^{2-} + HCl \xrightarrow{phenolphthalein} HCO_3{}^- + Cl^- \quad (2)$$

$$HCO_3{}^- + HCl \xrightarrow{methyl\ orange} CO_2\uparrow + H_2O + Cl^- \quad (3)$$

2. The Winkler method[19] is used to determine the concentration of initial hydroxide and bicarbonate in the solution. Excess KOH solution is added, which reacts with the bicarbonate in the solution to form carbonate. This is followed by the addition of excess 10%$BaCl_2$ forming $BaCO_3$, as a precipitate.

$$OH^- + OH^-{}_{excess} + HCO_3{}^- \rightarrow CO_3{}^{2-} + OH^-{}_{unreacted} + H_2O \quad (4)$$

$$CO_3{}^{2-} + BaCl_2 \rightarrow BaCO_3\downarrow + 2Cl^- \quad (5)$$

$$OH^-{}_{unreacted} + HCl \xrightarrow{phenolphthalein} H_2O + Cl^- \quad (6)$$

3. The $BaCl_2$ method is used to determine hydroxide concentration. Excess 10% $BaCl_2$ is directly added to the solution precipitating carbonate ions. The hydroxide concentration in the membrane is determined by titrating it with HCl and the bicarbonate remains unchanged as it only neutralizes below pH 8 to liberate CO_2.

$$CO_3{}^{2-} + BaCl_2 \rightarrow BaCO_3\downarrow + 2Cl^- \quad (7)$$

$$OH^- + HCl \xrightarrow{phenolphthalein} H_2O + Cl^- \quad (8)$$

So overall, we have three unknowns (OH^-, CO_3^{2-} & HCO_3^-) and three equations to evaluate the concentration of each species.

The equations are as follows:

$$V_{HCl1} = V(OH^-)_m + V(HCO_3{}^-)_m + V(CO_3{}^{2-})_m \quad (9)$$

$$V_{HCl2} = V(OH^-)_{excess} + V(OH^-)_m - V(HCO_3{}^-)_m \quad (10)$$

$$V_{HCl3} = V(OH^-)_m \quad (11)$$

Here, $V_{HCl\ 1,2,3}$: mmol of HCl required for titration 1,2, and 3. V (OH^-, HCO_3^-, and CO_3^{2-})$_m$: mmol of OH^-,HCO_3^-, and CO_3^{2-} in the membrane. V(OH^-)$_{excess}$: mmol of excess KOH added to convert HCO_3^- into CO_3^{2-} so it could be precipitated by adding excess $BaCl_2$. The 3rd titration was validated in a CO_2 free glove-bag to confirm its accuracy. Later, stock mixtures of OH^-, CO_3^{2-}, and HCO_3^- in a specific ratio were prepared in the glove bag and all three titrations were performed.

Transient conductivity measurement (in plane)

Samples in the pure HCO_3^- form were prepared as described above and loaded into a BekkTech conductivity cell.[15] Using method described by Ziv et al, HCO_3^- form was converted to OH^- form.[30] The cell was equilibrated in UHP N_2 and switched to ambient air (400 ppm CO_2) and then their ionic conductivities measured on exposure to air at 60 °C, and 75 or 85% RH. The ionic conductivity was measured every 4 minutes using electrochemical impedance spectroscopy to obtain the ionic resistance. The conductivity is given by the formula:

$$\sigma = d/ (t \times W \times R) \quad (12)$$

where, d is the distance(cm) between two inner platinum electrodes, t and W are the thickness(cm) and width(cm) of the sample respectively and R is the ionic resistance of the sample. To study the transient behaviour, the statistical average of all air cycles was plotted separately.

Transient change in mass when exposed to air

We used Dynamic Vapor Sorption (Surface Measurements, DVS Advantage 1) for gravimetric weight measurement. Membrane samples were in the weight range of 10-20 mg. After soaking in 1M KOH and washing with degassed DI water for 24 h, the samples were loaded on to the measurement pan.

Small and Wide-angle x-ray scattering (SAXS/WAXS):

Small-angle x-ray scattering was performed at the Basic Energy Sciences Synchrotron Radiation Center, beamline 12-ID-B/C/D of the Advanced Photon Source at Argonne National Laboratory. The beam energy was fixed at 13.3 or 14 keV and a Pliatus 2M SAXS detector was used to collect the data. Initially the samples were soaked in 1M KOH and washed with degassed DI water in a CO_2 free N_2 environment glovebox. The prepared samples were then loaded in the custom-built environmental chamber under a CO_2 free atmosphere by attaching the glove-bag to the chamber. The detailed procedure is explained in a previous work.[27] The samples were equilibrated with UHP Ar at 60 °C and a fixed humidity condition for 1 h and then the inlet gas was switched to compressed air (400 ppm CO_2). The temperature and humidity were controlled using Labview® program, details have been explained in previous work.[31]

Membrane electrode assembly (MEA) fabrication

The Gas Diffusion Electrodes(GDEs) were prepared by hand spraying a catalyst layer onto a gas diffusion layer (GDL, Toray TGP-H-060 with 5% PTFE wet proofing).[7] The PFAEM solid ionomer was ground finely with a mortar and pestle, followed by mixing with Pt on Vulcan carbon (Alfa Aesar HiSPEC 4000). Then, a small amount of DI water (1 ml) was added to the solid mixture and the mixture was ground for an additional 10 min to avoid aggregating the particles. The mixture was transferred to a vial. Then, 2-propanol was added (a total of 9 ml) to the mortar to rinse the residue and transferred to the mixture. Addition of 2-propanol to the mortar was repeated 2-3 times to ensure most of the ink mixture was collected. The final ground ink mixture was tip sonicating for 20 seconds and then bath sonicated in an ice bath for 20 min before it was hand sprayed onto the Toray GDL to produce one 25 cm^2 GDE. The average platinum

catalyst loading of these GDEs was 0.485 ± 0.05 mg cm^{-2}, determined by X-ray fluorescence (XRF). Two 5 cm^2 GDEs (anode and cathode electrodes, respectively) were cut to assemble with an over-sized 5 cm^2 PF AEM to make an MEA.

Before the GDEs and the anion exchange membrane were assembled for fuel cell testing. Both GDEs and membranes were exchanged in 1M KOH solution for a total of 60 minutes with replacing new base solution every 20 minutes. The membrane was sandwiched between two GDEs and pressed together and secured in a 5 cm^2 Fuel Cell Technologies hardware between two single pass serpentine flow graphite plates using PTFE gaskets to obtain a 25% compression with 20% pinch (5.1Nm torque).

Fuel Cell Testing

The fuel cell was assembled and then the cell temperature and anode-cathode dew point were set at 60 °C. H_2 and N_2 were flowed through the anode and cathode, respectively, until the desired temperature was achieved. Then the N_2 was switched to O_2 on the cathode and current was pulled through the cell and allowed to break-in at a constant voltage of 0.5V. After 2 h, the anode/cathode dew-point was lowered to 57 °C so that the relative humidity of the inlet gas in both compartments was 85%RH. After the cell was equilibrated at this temperature, a voltage polarization curve was obtained by sweeping voltage from OCV to 0.1 V. After the polarization curve, the cell was held at a constant voltage of 0.6V. Then the cathode inlet gas was switched from O_2 to clean air (<5 ppm CO_2). After the current density was equilibrated, a voltage polarization curve was evaluated. Then the cell was held at a constant voltage of 0.6V and exposed to air (400ppm CO_2). The cell performance was monitored over time until it reached equilibrium.

After equilibrium the self-purging of the cell was studied by ramping the cell down from OCV to 0.2 V. The cell was equilibrated at each voltage value to study the change in current density over time.

Results and Discussion:

Transient change in mass when exposed to air:

From Fig. S1(a) ESI (‡) we observe that the weight of the OH^- form sample immediately increases when exposed to air containing 400 ppm CO_2. Bharath VJ et al. have studied the change in mass of the Tokuyama A201 membrane as it is exposed to ambient air with CO_2.[32] The mass change was obtained using a QCM and they have also reported that the mass increases as the CO_2 reaction proceeds.

Our previous data suggest that the water uptake (λ) quantity changes with the ionic forms as follows: OH^- > air exposed OH^-(which mainly consists HCO_3^- & CO_3^{2-}) for PFAEMs.[33] Marino et al. and Jing et al. have also observed this behavior previously.[17, 34] Therefore, when we expose the sample to air we should expect to see a drop in weight of the sample as the water is lost. However, our results are counter-intuitive. The reason we see a rise in weight is that λ is a relative quantity, which is dependent and calculated using the dry mass of the sample. Therefore, when we compare two ionic form (OH^- & HCO_3^-/CO_3^{2-}) data we should also consider that the inherent dry mass is different for both forms. Therefore, we can conclude that the dry mass of HCO_3^-/CO_3^{2-} form is higher than the OH^- form.

The mass approaches equilibrium value in 15 min, which is equivalent to the CO_2 absorption and the slow-time constant, observed in the conductivity data, discussed below. This time can also be related to consumption of OH^- observed from the concentration profile. It should also be noted that HCO_3^- form when exposed to pure N_2 (0 ppm CO_2) it mostly converts back to OH^- which is evident from the water uptake data in Fig. S1(b) ESI (‡) and conductivity data in fig.2. This is because HCO_3^- is in equilibrium with OH^- and CO_2 and as per Le Chatelier's principle when exposed to no CO_2 condition the equilibrium will shift to OH^- predominantly and CO_2 will liberate through the chamber exhaust.

Transient Ionic conductivity when exposed to air:

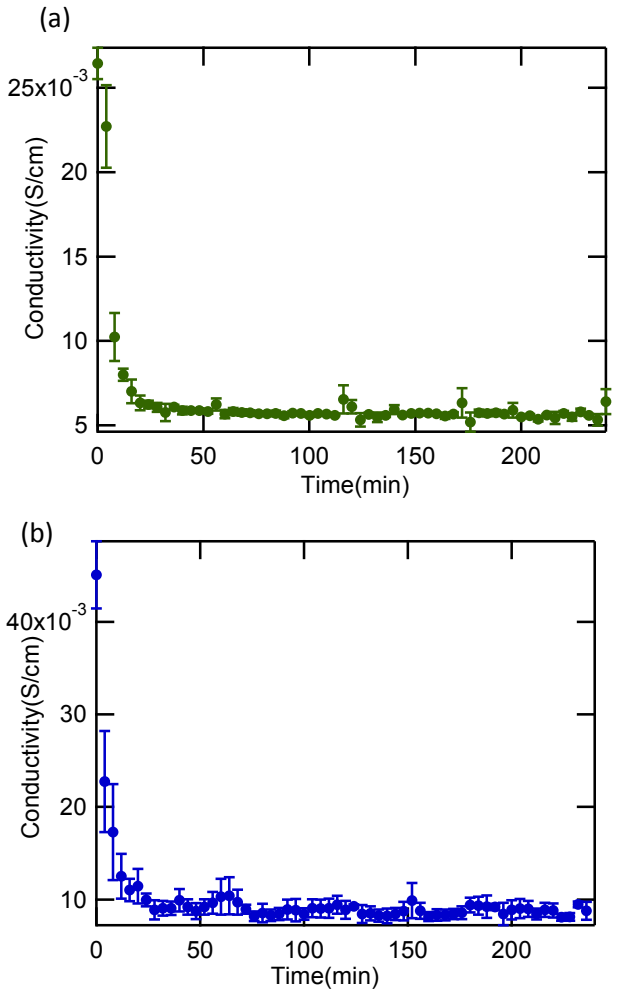

Fig.1: Transient conductivity change when a pure OH^- form of the PFAEM is exposed to ambient air containing 400 ppm CO_2 at 60 °C and (a) 75%RH and (b) 85%RH.

The fall in ionic conductivity of the PFAEM in the hydroxide form when exposed to air at 75 and 85% RH is shown in Figure 1. The data shown in Figure 1 was fit to a double exponential equation to analyze

the equilibration constants, however the slow time constant shows significant deviation. The conductivity of the membrane in OH^- form is 26 and 45 mS/cm at 75 & 85%RH respectively. The drop happens very quickly to 5 and 8 mS/cm at 75 & 85%RH respectively within 20 mins. Ziv et al. also observed that the drop in conductivity happens within 20 min for the studied hydrocarbon membranes.[35]

It should also be noted that the conductivity of the air-equilibrated carbonated sample can be recovered when exposed to gas containing no CO_2.[36] We have observed similar behavior with the PFAEMs and the results are shown in Figure 2. Cycles of air exposure followed by CO_2 free N_2 are shown, and the conductivity is fully recovered after each cycle in 48 h.

Transient SAXS

Figure 3 shows the transient SAXS data for the uptake of CO_2 to the hydroxide form of the PFAEM. From figure 3 a, b and c we observe that there are two prominent features in the SAXS data at q~0.06 and q~0.15 $Å^{-1}$. As the precursor of the studied membranes is perfluorinated sulfonyl fluoride of the 3M ionomer, the former broad feature corresponds to the intercrystalline spacing between the crystalline domains of the PTFE backbone, i.e. the matrix knee, and the feature at larger q is associated with ionic domains which is the mean correlation spacing between the hydrophilic water domains of the polymer.[37, 38] As the CO_2 from the air reacts with the OH^- ions in the films, we observe a drop in intensity of the scattering over time (Fig S2 a,b,c) ESI(‡). The ionomer feature (q~0.12-0.15) slightly shifts to the larger q over time indicating that there is a drop in the d-spacing of the feature due to water loss. It has been reported in the literature that OH^- form of AEMs have higher number of water molecules per cation, λ, as compared to HCO_3^- or CO_3^{2-} forms of these films.[17, 33, 34] Loss of water also leads to a drop in intensity of the ionomer domain feature. We also observe that the time of equilibration is faster at lower %RH, ca. 2h 20min (50%RH), 6h (75%RH) and 17h (85%RH).

The porod slope of the scattering data becomes more negative as the reaction proceeds which might suggest it's tending towards a more symmetrical maybe even spherical morphology for the wetter sample at 75% RH, Table 1.[26, 38] However, it should be noted that perfluorinated type membranes have a very complicated morphology.[27] The data could be fit to a double exponential mathematical equation,

$$I(a.u) = I_0 + A_1 e^{-\left(t - t_0 / \tau 1\right)} + A_2 e^{-\left(t - t_0 / \tau 2\right)} \quad (13)$$

Here, we are mainly interested in the fast and the slow time constants of the data. Except for the 85%RH data, the drop in intensity perfectly fits the double exponential equation. The time constants from the data fit shown in [Fig. S2 a, b and c] ESI (‡) are shown in Table 2. At 50% RH the short and long-time constants are 9.6 and 58.3 min respectively and at 75%RH much longer 23.4 and 168.3 min respectively. From the data, we can infer that the membrane goes through two distinct morphological changes sequentially as it goes from OH^- to the CO_3^{2-}/HCO_3^- form, before it achieves equilibrium.

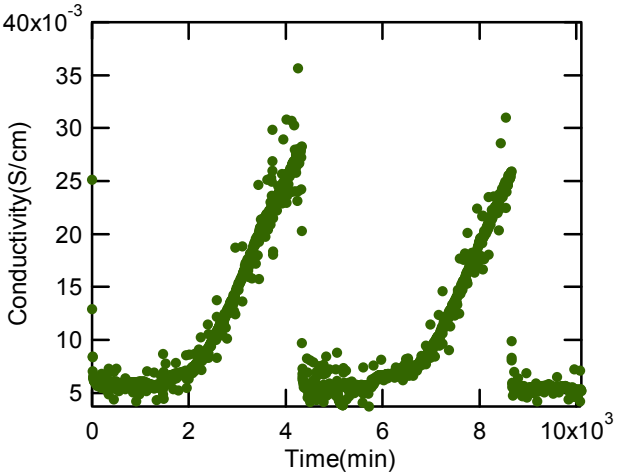

Fig. 2: Transient change in conductivity of the PFAEM at 60 °C and 75%RH when inlet gas is switched from compressed air (400 ppm CO_2) to UHP N_2 and back to air again.

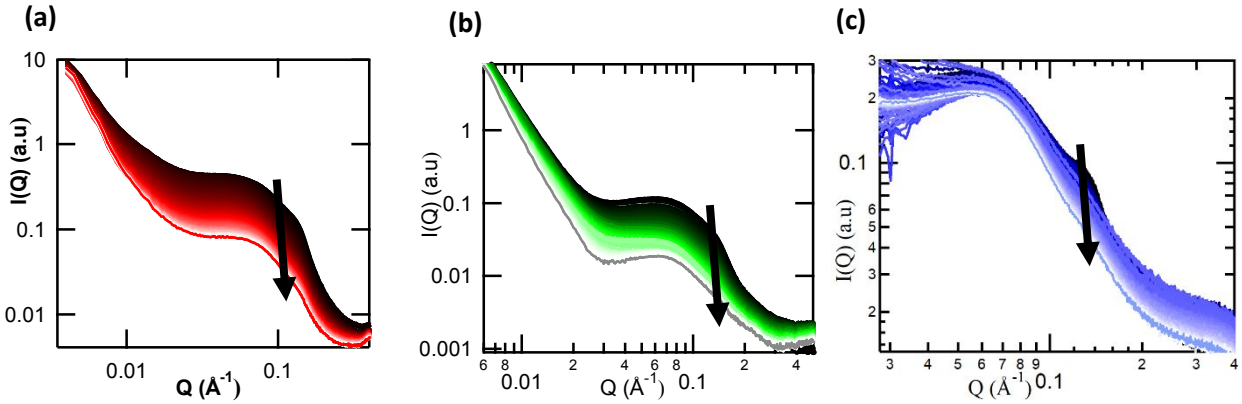

Figure.3: Transient small-angle x-ray scattering data of PFAEM equilibrated using UHP Ar and then exposed to compressed air (400 ppm CO_2) at 60 °C and (a)50%,Fig adaptation,[33] (b) 75% and (c) 85%RH.

The fast time constant is likely due to sudden drop in water content as the OH^- ions convert to HCO_3^-/CO_3^{2-} which is evident from conductivity and mass change shown previously whereas the slow time constant could be the sequential slow relaxation of polymer chains due to shift in ionic chemistry as it reaches equilibrium.

%RH	Porod slope		Porod range (nm)
	$T_{initial}$	$T_{equilibrium}$	
50	-2.6	-3.5	66-140
75	-3.4	-4.4	36-157

Table 1: Initial and equilibrium porod slope of SAXS data.

Time constants	%RH	τ1	τ2
SAXS	50	9.6 ± 0.4	58.3 ± 3
	75	23.4 ± 1.7	168.3 ± 9
	85	Data too noisy	
WAXS	50	17.4 ± 0.8	130 ± 18
	75	37 ± 7	258 ± 54
	85	48.6 ± 13	805 ± 60

Table 2: Time constants of conductivity, ionomer feature intensity (SAXS) and inter-chain feature intensity (WAXS) vs time of exposure to air (400 ppm CO_2).

Wide angle x-ray scattering:

The WAXS data shown in figure 4 a, b and c shows that two major feature peaks at q~1.2 and 2.6 $Å^{-1}$ are observed. The low q feature data can be fit to 3 gaussians (figure 4 d, e and f) which represent one distinct amorphous peak at q~1.1 $Å^{-1}$ and a super-imposed crystalline peak at q~1.2 $Å^{-1}$ which corresponds to inter-chain CF_2-CF_2 spacing of the fluorocarbon PTFE backbone of the polymer.[37] These super-imposition of two gaussian peaks have also been discussed in the Nafion® literature, a similar perfluorinated sulfonic acid polymer with a PTFE backbone and a longer sulfonated side chain than in this polymer.[39] Apart from these two gaussian peaks, there is one more Gaussian peak observed at q~1.5 $Å^{-1}$ which has also been observed in PFSA WAXS literature.[40] The peak observed at q~2.6 $Å^{-1}$ and is assigned to the intra-chain distance of fluorocarbon.[41] But due to limitations of beamline data window the feature was not entirely represented in the data. As the CO_2 reaction proceeds the inter-chain feature becomes flatter. The intensity of inter-chain peak at q~1.2 $Å^{-1}$ also follows a double-exponential drop behavior (Fig. S3: a, b & c) ESI (‡) and the time constants are in Table 1. The time of equilibration is higher at the higher humidity similar to SAXS data, but at much longer times.

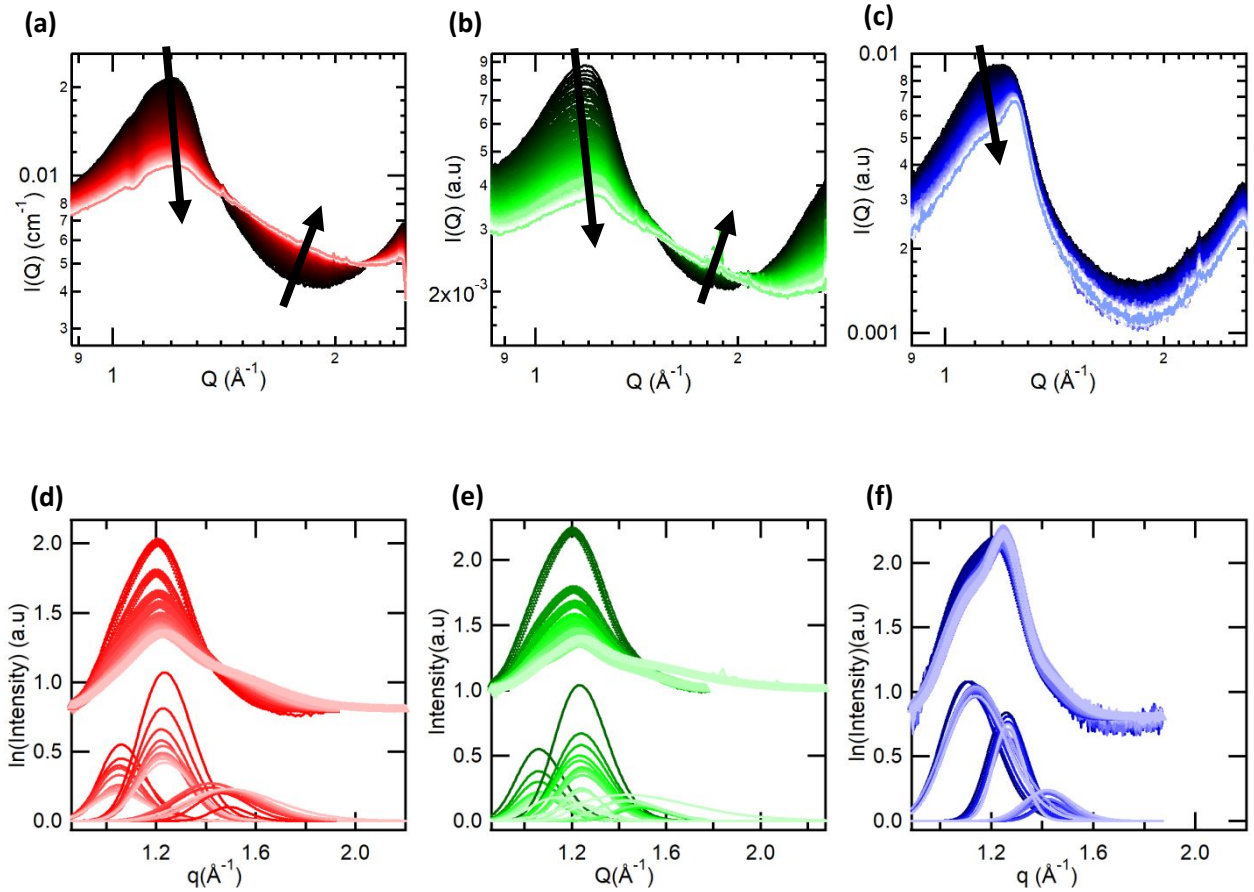

Figure 4: Transient wide-angle x-ray scattering data of PFAEM Gen2 polymer equilibrated using UHP Ar and then exposed to compressed air (400 ppm CO_2) at 60 °C and (a) 50%, (b) 75% and (c) 85%RH. Gaussian fits of inter-chain feature observed at (d) 50%, (e) 75% and (f) 85%RH.

The transient data was fit to 3 Gaussians (figure 4 d, e, and f) to understand the evolution of features and the effect of the CO_2 reaction on their area, height and width. The change in the width of the Gaussian peaks of the WAXS data is not that significant. The crystalline inter-chain peak at q~1.2 $Å^{-1}$ and amorphous peak at q~1.1 $Å^{-1}$ drops in intensity and area over time [Fig. S4: a, b, & c; Fig. S5: a, b, c, d, e, & f] ESI (‡). Simultaneously, the peak observed at q~1.5 $Å^{-1}$ rises over time. This indicates that the membrane is losing crystallinity as it goes from single ion OH^- form to the mixed ions of the HCO_3^-/CO_3^{2-} form.

Titration methodology:

We attempted to use a new titration methodology to evaluate the concentrations of all three species simultaneously. The carbonate/bicarbonate reactions are as follows:

$$OH^- + CO_2 \rightarrow HCO_3^- \quad (14)$$

$$HCO_3^- + OH^- \rightarrow CO_3^{2-} + H_2O \quad (15)$$

Results from the Warder titration give us equation 9 with 3 ions (OH^-, CO_3^{2-} & HCO_3^-) as variables. Winkler's method that has 2 ions (HCO_3^- & OH^-) in equation 10 was then used. And finally, adding $BaCl_2$ to the ionic mixture gives us equation 11 with just the OH^- ion.[42] By solving the three equations simultaneously we can calculate the concentrations of all 3 species (OH^-, CO_3^{2-} & HCO_3^-). To the author's knowledge the 3rd titration lacks experimental evidence and has been very vaguely reported in the literature.[42] Therefore, some experiments were conducted to confirm its validity. The titration is 95 to 99% accurate when performed under CO_2 free condition and in the absence of carbonate species as mentioned in [Fig S6(a)] ESI (‡). The equilibrium values obtained from the titration of custom-made ionic mixtures (OH^-, CO_3^{2-} & HCO_3^-) tend to deviate from the actual mixing concentrations as OH^- & HCO_3^- react to form CO_3^{2-}. As shown in the [Fig. S6(b)] ESI (‡), the residual OH^- left in the actual solution is less than its concentration before mixing with CO_3^{2-}/HCO_3^-. We notice that for fractions <0.3, OH^- is practically undetectable which is because it has completely reacted with HCO_3^-. The deviation detected indicates that this is only a qualitative proof of co-existence of the three anionic species. A more sophisticated modelling of the species equilibrium will need to be done before making any quantitative conclusions about the species kinetics.

Species concentration profile:

The experiment was carried out at room conditions with only exception of PFAEM which was done at 30 °C and 95%RH. In the previous literature it was stated that the CO_2 reaction with OH^- is dependent on the conditioning of AEM as it is exposed to air.[8] Yanagi and Fukuta exposed the commercial Tokuyama A201 film under wet conditions and report that the OH^- ions deplete within 30 min where $\lambda = 9.2$ and an IEC = 1.5.[15] Kizewski et al. have reported that OH^- gets depleted within an hour, for a radiation grafted AEM where $\lambda = 22$ and an IEC = 1.4.[16] Whereas, Marino and Kreur used a high water content uncross-linked FAA-3 membrane and report that it takes ~100 min for OH^- to react with CO_2 and deplete to a OH^- of <10% IEC, where $\lambda = 100$ and an IEC = 2.1.[17] By comparing the time of depletion observed in different studies we can conclude that the amount of water and the ionic capacity of the membrane plays a significant role in rate of OH^- depletion (figure 5). The concentration profile studies of Maes et al. obtained transient FTIR spectrum when an OH^- form of a chlorinated poly(propylene) aminated with branched poly(ethyleneimine) AEM is exposed to ambient air they identified two different C-O stretches at 1380 and 1460 cm^{-1} which correspond to formation of bicarbonate and carbonate ions respectively.[26] The area under each peak was calculated and plotted vs time and it was noticed that the bicarbonate grows more intense than the carbonate. As the OH^- ions react, HCO_3^- and CO_3^{2-} ions are formed simultaneously.

We tested the membranes by exposing them to air at a fixed temperature of 60 °C and different relative humidity conditions as shown in [Fig. S7: a, b, & c] ESI (‡). Here we observe that the OH^- ions react slowly at the higher humidity condition, 85% RH, but for all humidity conditions the hydroxide charge carrier depletes within ca. 20 min for the PFAEM, which has a $\lambda = 9$ and an IEC = 0.75 mmol/g. Comparing this result to two commercial films and another well characterized experimental film, Figure 6, we see that this theory is borne out. Most previous studies have reported that HCO_3^- ions are the dominant species at equilibrium.[15-17] A modelling study supports our results and it concludes that air-exposed OH^- AEM should have CO_3^{2-} as a dominant species at equilibrium.[43] A detailed fuel cell modelling studies suggests that at lower current density CO_3^{2-} is the most dominant species in an active fuel cell.[44, 45] Also, another plausible explanation is that the CO_3^{2-} ions favor more basic environment compared to HCO_3^-. As the membrane is exposed for a certain time and further soaked in 1M KCl for ion exchange, the species internally reach an equilibrium as explained in titration

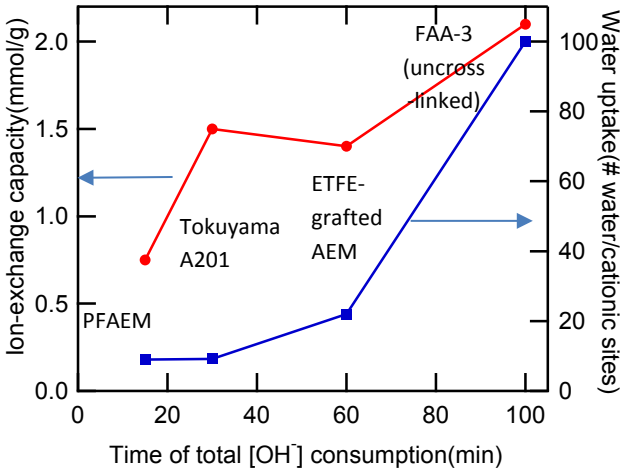

Fig.5: Ion-exchange capacity(circles) and water content(λ)(squares) vs time of OH^- charge carrier depletion for the PFAEM (this study), a commercial hydrocarbon AEM, Tokuyama A201, a radiation grafted ETFE AEM, and an uncross linked version of a second AEM, FAA-3.[15-17, 33]

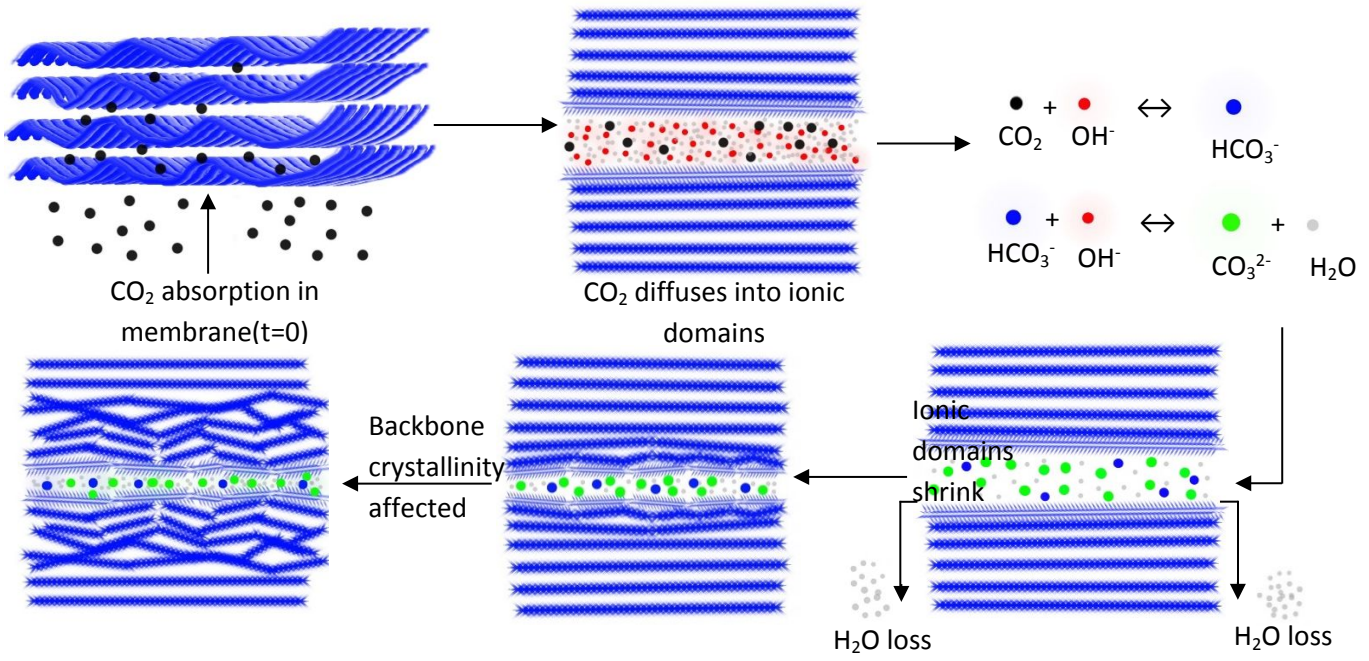

Fig 6: Schematic of carbon-dioxide absorption process and the down-stream effects on the membrane.

Therefore, the data obtained [Fig. S7: a, b, & c)] ESI (‡) from titration only gives us qualitative insight into the nature of species at any given point of time. Any quantitative conclusion needs further improvement in the data analysis of titrations, or a better technique to quantify the species concentration.

Summary of ex-situ characterization tests:

As shown in the cartoon (fig 6) the CO_2 first diffuses into the membrane. The reaction of OH^- with CO_2 leads to a change in 3 different sequential changes in membrane characteristics: conductivity, side-chain spacing and then backbone crystallinity. The shift in chemistry of ionic groups leads to loss of water as well as drop in ionic conductivity as the carbonate/bicarbonate groups are larger than hydroxide. This leads to a shrinkage of the ionic nano-channels which is observed from the shift in d-spacing of small-angle x-ray scattering data. And this shift in d-spacing also affects the polymer backbone crystallinity which is evident from the transient WAXS data where we see that the inter-chain CF_2 spacing feature becomes flatter due to a new feature. Therefore, the CO_2 reaction is not only affecting the conductivity but also affects the overall polymer morphology. The rate at which it is affected depends on the humidity of the environment. The OH^- depletes slower at high humidity condition as it's harder to get out. And, the ionic domains as well as polymer chains equilibrate slower. Therefore, for optimal performance the fuel cell should be operated at higher humidity condition at least on the cathode side. Therefore, from the knowledge gained from our ex-situ test the fuel cell tests were carried out at 85%RH on both cathode as well as anode compartments.

H_2/Air fuel cell data when switched from clean to ambient air:

The fuel cell performance at 0.6 V (current density) is shown in Fig. 7(a) which shows a drop in performance over ca. 14 h to ca. 300 mA/cm^2 from an initial value of ca. 900 mA/cm^2 when the cathode gas is switched from CO_2 free air (<3 ppm CO_2) to ambient air (~400 ppm CO_2). The formation of CO_3^{2-}/HCO_3^-, which has lower mobility rates leads to the drop in performance observed in Fig. 7 (a) and the rise in the stack resistance shown in [Fig. S8(a)] ESI(‡). The situation is more complicated as, it has been reported in the previous literature that the oxygen reduction kinetics in carbonate environment are not as good as in an hydroxide environment, because of ionic mass transport limitations.[46] It has also been reported that the O_2 solubility is lower in CO_3^{2-} electrodes which limits the oxygen reduction.[47] Yanagi et al. has reported that the accumulation of HCO_3^-/CO_3^{2-} ions causes higher over potential in the anode, which leads to a drop in performance.[25] This fuel cell was observed to equilibrate in 13-15 h, Figure 7(a), at 0.6 V, which is not totally consistent with other observations of similar AEM fuel cells. For example Piana et al. observed that the cell performance drops within minutes after being switched from clean air to ambient air.[48] However, it should be noted that they used catalyst-coated membrane (CCM) whereas for our test we used Gas-diffusion electrode (GDE).

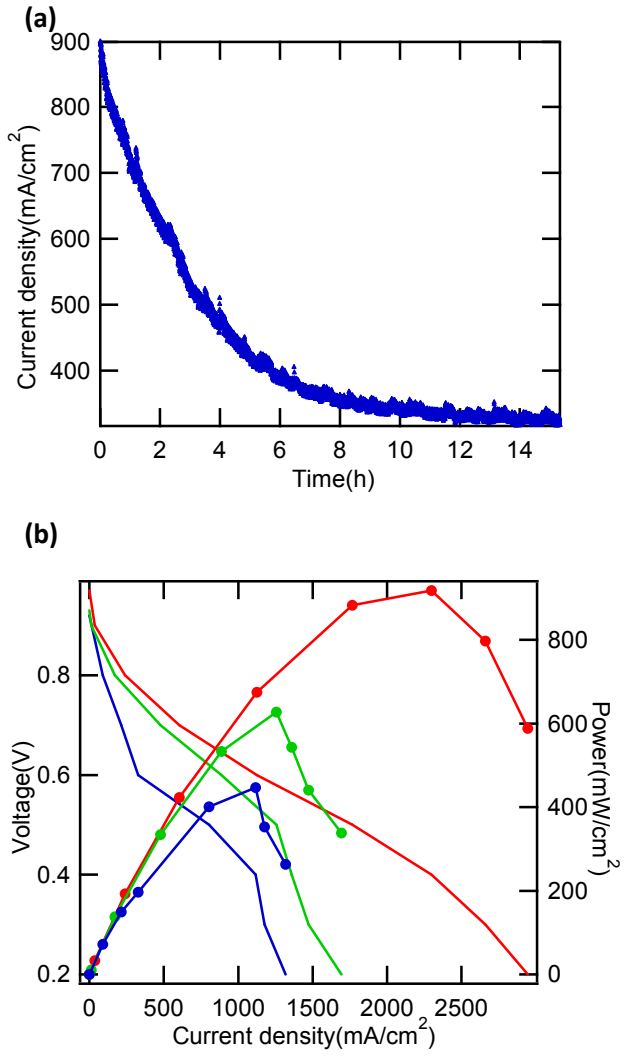

Fig.7: (a). Current density vs time when the fuel cell is switched from clean air to ambient air (400 ppm CO_2) (b) Voltage vs current density (solid line) and Power vs current density (solid line and markers in between) of a H_2/O_2 (red), H_2/clean air (green) and H_2/ambient air (blue).

Dekel et al. has also reported similar findings where the voltage drops instantly after switching to ambient air when held at a constant current density.[13] The reason our cell takes hours instead of minutes could be associated with the difference in polymer chemistry as well as fabrication method of the electrodes which uses powder grinding method which might lead to porosities different than a dispersion methodology electrode. Recently, Zheng et al. studied CO_2 related voltage loss using powder grinded electrodes in MEA.[49] Here, the voltage reaches equilibrium within minutes but it should be noted that anode and cathode are operated at much dryer conditions. This also supports our hypothesis that higher humidification affects carbonation in an AEMFC and hence the slow equilibrium. The cell was later taken to OCV and slowly the voltage was ramped down in steps to 0.6V. We observe that cell achieves equilibrium instantly [Fig. S8(b)] ESI (‡). Then, as soon as the cell is held at 0.5V we observe that the cell starts off at a current density and constantly increases over time [Fig. S8(c) ESI (‡)]. Simultaneously, the resistance is observed to go down [Fig. S8(d) ESI (‡)]. This is due to self-purging phenomenon of AEMFC when the HCO_3^-/CO_3^{2-} anions are converted to CO_2 and OH^- ions are formed.[50, 51] Pennline et al. has suggested that the self-purging ability of AEMFCs could be applied to CO_2 sequestration.[52] Gottesfeld et al. has reported that the ionic conductivity of the membrane increases with self-purging which would lead to a rise in performance.[13] In the literature it was suggested that the self-purging perfectly removes CO_2 from the cell when it is operated at current densities above 1000 mA/cm^2.[53] However, it's reported by Zheng et al. that the CO_2 related over-potential is still overwhelming at higher current density operation.[49] The fuel cell polarization curve is shown in fig. 7(b) using H_2/O_2, H_2/clean air (<3 ppm CO_2) and H_2/ambient air (400 ppm CO_2). The data points for ambient air were taken under equilibrium considering the self-purging phenomenon. The peak power performance of the fuel cell was observed to be 918, 627 and 446 mW/cm^2 for O_2, clean air and ambient air as cathode gas respectively. By comparing the polarization curve of clean air (<3 ppm CO_2) and O_2 we see mass transfer losses (drastic drop in limiting current density) by reducing the oxygen content however, the kinetics aren't substantially affected. But when we compare ambient air and clean air performance, we see a huge over-potential. It can be clearly seen that both the kinetic and mass transfer loses are dramatically affected by the presence of 400 ppm of CO_2.The polarization curve with ambient air shows the lowest performance, however, this is one of the highest ambient air performances that has been reported for an AEMFC so far. Clearly the kinetics of the electrode are reduced, by the presence of HCO_3^-/CO_3^{2-} anions which agrees with modelling results reported by Gerhardt et al.[54] Interestingly the IR portion of the curve is not so a badly affected implying that the major charge carrier in the AEM is hydroxide.

Conclusions

An AEM with a perfluorinated backbone was investigated to understand the effect of the 400-ppm carbon dioxide currently in ambient air on the physico-chemical, electrochemical, and morphological properties, as well as on the fuel cell performance. The anionic conductivity decays from 0.022 to 0.005 mS/cm and 0.045 to 0.008 S/cm in ca. 20 min which most likely corresponds to change in chemistry from highly mobile OH^- ion to HCO_3^-/CO_3^{2-} ions which have lower mobility. From the SAXS data we notice that the change in ionic chemistry causes the ionic domains in the polymer to shrink and to lose intensity due to loss of water. It takes ca. 2.5, 6 and 16 h to equilibrate the SAXS profile when the reaction is carried out at 50, 75 and 85%RH respectively. At longer times the ionic domains in the polymer rearrange and then finally we see a change in the polymer backbone crystallinity from the WAXS data. The height of the inter-chain feature observed at q~1.2 Å^{-1} is observed to reduce over time, while we see a change in the area of the entire feature. To understand this in detail we fit the data to Gaussian curves, and we

can conclude that the area and height of the inter-chain feature drops over time and another feature at intensity of q~1.5 $Å^{-1}$ builds up. Here, we notice that the time constants of WAXS are slightly higher than SAXS. A titration methodology was used to get qualitative insights into the nature of species present during CO_2 exposure. We observe that the OH^- consumption happens within 20 min and HCO_3^-/CO_3^{2-} are formed simultaneously, actual species concentration at the time of exposure is still unknown. So, if we compare all data, we can conclude that change in chemistry leads to sequential changes in the membrane properties as follows: anionic conductivity, ionic domains (SAXS) and backbone crystallinity (WAXS). From ex-situ tests we learn that the membrane properties are more retained and affect slowly when the reaction happens at higher humidity condition as it's difficult for water to leave. And therefore, we did in-situ fuel cell tests at higher humidity condition of 85%RH. We see that the current density drops over time as the cathode gas is changed from clean air (< 3 ppm CO_2) to ambient air (400 ppm CO_2) in 13-15 h for the cell to equilibrate. We studied the self-purging phenomenon of CO_2 after the cell was fully equilibrated and the peak power data is one of the highest reported performances for H_2/ ambient air fuel cell system, 446 mW/cm^2. From this study we can conclude that operating the fuel cell at high humidity will be beneficial as OH^- depletes slower, presence of CO_3^{2-} /HCO_3^- significantly affect anode kinetics, and hence the difference in performance between clean air and ambient air.

Conflicts of interest

There are no conflicts to declare.

Acknowledgements

The work was supported by the U.S. Department of Energy under Contract No. DE-AC36-08GO28308 with Alliance for Sustainable Energy, LLC, the Manager and Operator of the National Renewable Energy Laboratory. Funding provided by the U.S. Department of Energy Office of Energy Efficiency and Renewable Energy Fuel Cell Technologies Office. The views and opinions of the authors expressed herein do not necessarily state or reflect those of the United States Government or any agency thereof. Neither the United States Government nor any agency thereof, or any of their employees, makes any warranty, expressed or implied, or assumes any legal liability or responsibility for the accuracy, completeness, or usefulness of any information, apparatus, product, or process disclosed, or represents that its use would not infringe privately owned rights. The U.S. Government retains and the publisher, by accepting the article for publication, acknowledges that the U.S. Government retains a nonexclusive, paid-up, irrevocable, worldwide license to publish or reproduce the published form of this work, or allow others to do so, for U.S. Government purposes. This research used resources of the Advanced Photon Source, a U.S. Department of Energy (DOE) Office of Science User Facility operated for the DOE Office of Science by Argonne National Laboratory under Contract No. DE-AC02-06CH11357.

Notes and references

1. J. R. Varcoe, P. Atanassov, D. R. Dekel, A. M. Herring, M. A. Hickner, P. A. Kohl, A. R. Kucernak, W. E. Mustain, K. Nijmeijer, K. Scott, T. Xu and L. Zhuang, *Energy & Environmental Science*, 2014, **7**, 3135-3191.
2. E. Agel, J. Bouet and J. Fauvarque, *Journal Of Power Sources*, 2002, **105**, 87-87.
3. Varcoe, Jr., R. Slade, G. Wright and Y. Chen, *Journal Of Physical Chemistry B*, 2006, **110**, 21041-21049.
4. D. R. Dekel, *Journal of Power Sources*, 2017, **375**, 158-169.
5. J. Zhou, M. Unlu, J. A. Vega and P. A. Kohl, *Journal of Power Sources*, 2009, **190**, 285-292.
6. C. M. Lang, K. Kim and P. A. Kohl, *Electrochemical and Solid-State Letters*, 2006, **9**, A545-A548.
7. T. J. Omasta, A. M. Park, J. M. Lamanna, Y. Zhang, X. Peng, L. Wang, D. L. Jacobson, J. R. Varcoe, D. S. Hussey, B. S. Pivovar and W. E. Mustain, *Energy & Environmental Science*, 2018, **11**, 551-558.
8. N. Ziv, W. E. Mustain and D. R. Dekel, *Journal*, 2018, **11**, 1136-1150.
9. G. Li, Y. Wang, J. Pan, J. Han, Q. Liu, X. Li, P. Li, C. Chen, L. Xiao, J. Lu and L. Zhuang, *International Journal of Hydrogen Energy*, 2015, **40**, 6655-6660.
10. C. G. Arges and L. Zhang, *ACS Applied Energy Materials*, 2018, **1**, 2991-3012.
11. G. Merle, M. Wessling and K. Nijmeijer, *Journal of Membrane Science*, 2011, **377**, 1-35.
12. A. G. Divekar, B. S. Pivovar and A. M. Herring, *ECS Transactions*, 2018, **86**, 643-648.
13. S. Gottesfeld, D. R. Dekel, M. Page, C. Bae, Y. Yan, P. Zelenay and Y. S. Kim, *Journal of Power Sources*, 2018, **375**, 170-184.
14. G. B. Peter, A. F. Stefan, J. H. Laurence and T. Jean-Marie, *Nature Materials*, 2011, **11**, 19-29.
15. H. Yanagi and K. Fukuta, *ECS Transactions*, 2008, **16**, 257-262.
16. J. Kizewski, N. Mudri, R. Zeng, S. Poynton, R. C. T. Slade and J. R. Varcoe, *ECS Transactions*, 2010, **33**, 27-35.
17. M. G. Marino, J. P. Melchior, A. Wohlfarth and K. D. Kreuer, *Journal of Membrane Science*, 2014, **464**, 61-71.
18. S. Suzuki, H. Muroyama, T. Matsui and K. Eguchi, *Electrochimica Acta*, 2013, **88**, 552-558.
19. A. I. Vogel, *Vogel's textbook of quantitative chemical analysis*, ed. G.H. Jeffery, J. Bassett, J. Mendham, R. C. Denney, John Wiley & Sons, New York, 5th ed., 1989,ch 10, 297-299.
20. E. T. Mark, M. Dominik and P. Michele, *Nature*, 2002, **417**, 925-929.
21. A. Amel, N. Gavish, L. Zhu, D. R. Dekel, M. A. Hickner and Y. Ein-Eli, *Journal of Membrane Science*, 2016, **514**, 125-134.
22. H. N. Sarode, Y. Yang, A. R. Motz, Y. Li, D. M. Knauss, S. Seifert and A. M. Herring, *The Journal of Physical Chemistry C*, 2017, **121**, 2035-2045.
23. T. D. Myles, K. N. Grew, A. A. Peracchio and W. K. S. Chiu, *Journal of Power Sources*, 2015, **296**, 225-236.
24. T. P. Pandey, A. M. Maes, H. N. Sarode, B. D. Peters, S. Lavina, K. Vezz, Y. Yang, S. D. Poynton, J. R. Varcoe, S.

Seifert, M. W. Liberatore, V. Di Noto and A. M. Herring, *Physical Chemistry Chemical Physics*, 2015, **17**, 4367-4378.
25. M. Inaba, Y. Matsui, M. Saito, A. Tasaka, K. Fukuta, S. Watanabe and H. Yanagi, *Electrochemistry*, 2011, **79**, 322-325.
26. A. M. Maes, T. P. Pandey, M. A. Vandiver, L. K. Lundquist, Y. Yang, J. L. Horan, A. Krosovsky, M. W. Liberatore, S. Seifert and A. M. Herring, *Electrochimica Acta*, 2013, **110**, 260-266.
27. A. G. Divekar, M.-C. Kuo, A. M. Park, A. R. Motz, Z. S. Page-Belknap, Z. Owczarczyk, H. Long, S. Seifert, C. M. Maupin, M. A. Yandrasits, Y. Yang, B. S. Pivovar and H. A. M., *Journal of Polymer Science: Part B*, 2019, **57**, 700-712.
28. A. M. Park, Z. R. Owczarczyk, L. E. Garner, A. C. Yang-Neyerlin, H. Long, C. M. Antunes, M. R. Sturgeon, M. J. Lindell, S. J. Hamrock, M. Yandrasits and B. S. Pivovar, *ECS Transactions*, 2017, **80**, 957-966.
29. L. Greenspan, *JOURNAL OF RESEARCH of the National Bureau of Standards- A. Physics and Chemistry*, 1977, **81 A**, 89-96.
30. N. Ziv and D. R. Dekel, *Electrochemistry Communications*, 2018, **88**, 109-113.
31. M. A. Vandiver, J. L. Horan, Y. Yang, E. T. Tansey, S. Seifert, M. W. Liberatore and A. M. Herring, *Journal of Polymer Science Part B: Polymer Physics*, 2013, **51**, 1761-1769.
32. V. J. Bharath, J. R. Jervis, J. J. Bailey, E. Engebretsen, T. P. Neville, J. Millichamp, T. Mason, P. R. Shearing, R. J. C. Brown, G. Manos and D. J. L. Brett, *International Journal of Hydrogen Energy*, 2017, **42**, 24301-24307.
33. A. G. Divekar, A. M. Park, Z. R. Owczarczyk, S. Seifert, B. S. Pivovar and A. M. Herring, *ECS Transactions*, 2017, **80**, 1005-1011.
34. J. Peng, A. L. Roy, S. G. Greenbaum and T. A. Zawodzinski, *Journal of Power Sources*, 2018, **380**, 64-75.
35. N. Ziv, A. N. Mondal, T. Weissbach, S. Holdcroft and D. R. Dekel, *Journal of Membrane Science*, 2019, **586**, 140-150.
36. T. Kimura and Y. Yamazaki, *Electrochemistry*, 2011, **79**, 94-97.
37. A. Kusoglu and A. Z. Weber, *Chemical reviews*, 2017, **117**, 987-1104.
38. Y. Liu, J. Horan, G. Schlichting, B. Caire, M. Liberatore, S. J. Hamrock, G. Haugen, M. A. Yandrasits, S. Seifert and A. Herring, *Macromolecules*, 2012, **45**, 7495-7503.
39. P. C. van der Heijden, L. Rubatat and O. Diat, *Macromolecules*, 2004, **37**, 5327-5336.
40. G. A. Giffin, G. M. Haugen, S. J. Hamrock and V. Di Noto, *Journal of the American Chemical Society*, 2013, **135**, 822-834.
41. H. Mendil-Jakani, S. Pouget, G. Gebel and P. N. Pintauro, *Polymer*, 2015, **63**, 99-107.
42. Manual on water, American Society for Testing and Materials, Philadelphia, 3rd ed., 1969, Ch. 10, 202-202.
43. K. N. Grew, X. Ren and D. Chu, *Electrochemical and Solid-State Letters*, 2011, **14**, B127-B131.
44. U. Krewer, C. Weinzierl, N. Ziv and D. R. Dekel, *Electrochimica Acta*, 2018, **263**, 433-446.
45. J. A. Wrubel, A. A. Peracchio, B. N. Cassenti, T. D. Myles, K. N. Grew and W. K. S. Chiu, *Journal of The Electrochemical Society*, 2017, **164**, F1063-F1073.
46. K. A. Striebel, F. R. McLarnon and E. J. Cairns, *Journal of the Electrochemical Society*, 1990, **137**, 3360-3367.
47. K. A. Striebel, F. R. McLarnon and E. J. Cairns, *Journal of the Electrochemical Society*, 1990, **137**,3351-3359.
48. M. Piana, M. Boccia, A. Filpi, E. Flammia, H. A. Miller, M. Orsini, F. Salusti, S. Santiccioli, F. Ciardelli and A. Pucci, *Journal of Power Sources*, 2010, **195**, 5875-5881.
49. Y. Zheng, T. J. Omasta, X. Peng, L. Wang, J. R. Varcoe, B. S. Pivovar and W. E. Mustain, *Energy & Environmental Science*, 2019, **12**, 2806-2819.
50. S. Watanabe, K. Fukuta and H. Yanagi, *ECS Transactions*, 2010, **33**, 1837-1845.
51. Z. Siroma, S. Watanabe, K. Yasuda, K. Fukuta and H. Yanagi, *Journal Of The Electrochemical Society*, 2011, **158**, B682-B689.
52. H. W. Pennline, E. J. Granite, D. R. Luebke, J. R. Kitchin, J. Landon and L. M. Weiland, *Fuel*, 2010, **89**, 1307-1314.
53. K. Fukuta, H. Inoue, S. Watanabe and H. Yanagi, *ECS Transactions*, 2009, **19**, 23-27.
54. M. R. Gerhardt, L. M. Pant and A. Z. Weber, *Journal of The Electrochemical Society*, 2019, **166**, F3180-F3192.

Graphical Abstract:

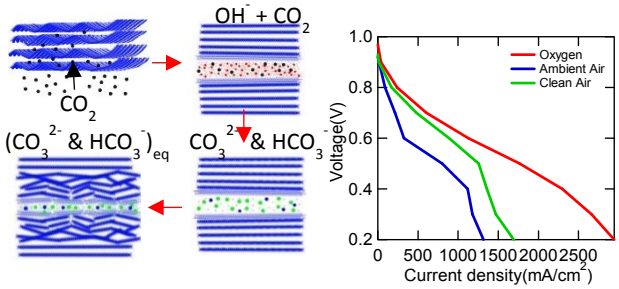

Text:

Ex-situ physico-chemical, electrochemical, and morphological analysis sheds light on CO_2 limitation of ambient air anion exchange membrane fuel cell.